ACS APPLIED POLYMER MATERIALS

pubs.acs.org/acsapm Article

Beta Phase Crystallization and Ferro- and Piezoelectric Performances of Melt-Processed Poly(vinylidene difluoride) Blends with Poly(methyl methacrylate) Copolymers Containing Ionizable Moieties

Alexandre De Neef, Cédric Samuel,* Harvey Amorín, Gregory Stoclet, Ricardo Jiménez, Philippe Dubois, Jérémie Soulestin, and Jean-Marie Raquez

Cite This: *ACS Appl. Polym. Mater.* 2020, 2, 3766−3780 Read Online

ACCESS | Metrics & More | Article Recommendations | Supporting Information

ABSTRACT: Poly(methyl methacrylate-*co*-methacrylic acid) (PMMA-*co*-MAA) copolymer containing ionizable moieties is here investigated as a melt processing additive for poly(vinylidene difluoride) (PVDF) to develop high-quality ferro- and piezoelectric polymer films by extrusion-calendering. The PVDF/PMMA-*co*-MAA miscibility and the β-phase crystallization from the melt state at high cooling rates were first explored by flash differential scanning calorimetry (FDSC). Transposition to the melt-processing of thin films by extrusion-calendering was attempted, and direct production of β-crystals in high amounts was confirmed at a specific content of 5 wt % PMMA-*co*-MAA. Ferro- and piezoelectric properties were subsequently investigated, and classical ferroelectric-type hysteresis loops clearly appeared at room temperature for AC electric fields higher than 900−1200 kV/cm. Enhanced remanent polarizations (P_r) were observed with only 5 wt % PMMA-based additives, and the best ferroelectric performances were identified for PVDF/PMMA-*co*-MAA blends, in agreement with a higher β-phase content. Stable piezoelectric properties are also highlighted with maximal piezoelectric coefficient (d_{33}) of 11 pC/N for these formulations. A linear relationship is found between d_{33} and P_r in accordance with several models, and in this respect, the origin and optimization of the remanent polarization was investigated. Crystal transformations were revealed during high-voltage AC poling, and high-quality ferroelectric behaviors with high P_r values up to 7 μC/cm^2 were obtained at elevated poling temperatures for PVDF/PMMA-*co*-MAA blends (theoretical d_{33} up to 16 pC/N) approaching the theoretical limit value for perfectly poled β-crystals. This study clearly opens up interesting perspectives in the development of cost-effective electroactive polymer films using industrially relevant processes and demonstrates that PVDF-based blends with miscible functional PMMA copolymers represent an interesting approach for this purpose.

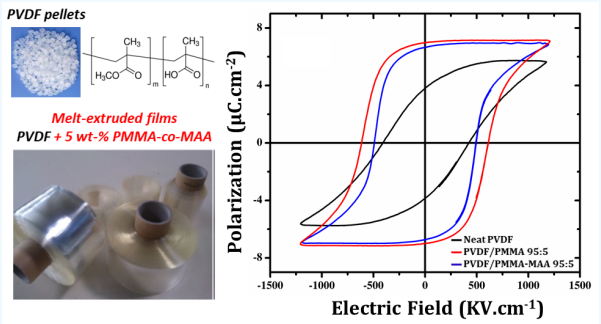

KEYWORDS: *poly(vinylidene difluoride), poly(methyl methacrylate), polymer blends, extrusion, piezoelectrics, ferroelectrics*

1. INTRODUCTION

For decades, high interest has been observed for the implementation of poly(vinylidene difluoride) (PVDF) and its copolymers in the domain of ferro- and piezoelectric materials.[1−4] Currently, ferroelectric and piezoelectric properties of PVDF-based materials are of great interest for flexible sensors, transducers, and actuators,[2−5] as well as for future prospects in many advanced applications such as energy harvesters or μ-generators,[6,7] energy storage,[8,9] random-access memories (FeRAMs),[10−12] artificial muscles for robotics, and (bio)microelectronic devices.[13]

The piezoelectric and ferroelectric properties of semicrystalline PVDF arise from specific crystalline phases depending on the conformation of the CH_2-CF_2 linkages.[1−4] Among the 3 main crystalline phases of PVDF, the most thermodynamically stable is the so-called α-phase (form II, conformation TGTG′),[1−4] which remains nonpolar with a paraelectric dielectric behavior. Unfortunately, this nonpolar phase is the most commonly produced during melt-state processing of PVDF. The other two phases are polar and of high interest for piezoelectric and ferroelectric properties, γ-phase (form III, conformation TTTGTTTG′) and β-phase (form I, conforma-

Received: April 2, 2020
Accepted: July 24, 2020
Published: July 24, 2020

tion 100% trans). This last conformation presents the highest dipolar moments, due to a regular arrangement of hydrogen and fluorine atoms in opposite directions resulting in a large molecular dipolar moment oriented perpendicularly to the chain axis. The parallel orientation of all the monomers in the β-phase allows reaching large spontaneous, remanent polarizations of 6.5−9 μC/cm^2, giving a maximum piezoelectric coefficient d_{33} of approximately 35 pC/N.[2−4,14−18] The amorphous phase and crystal−amorphous interphase from PVDF could play an important role in its electroactive properties in particular in charge transfer and coupling between crystalline lamellae.[19−21]

Unfortunately, the PVDF β-phase is difficult to obtain using a conventional melt-extrusion processing method and various approaches were developed. The most common route employed to get the PVDF β-phase is the uniaxial/biaxial stretching of PVDF films with a partial conversion of PVDF α-phase into the β-phase (efficiency close to 75−80%).[2,14,17] The PVDF β-phase could also directly appear from the melt state using specific (nano)fillers,[22−24] but conductive and non-polarizable PVDF materials are generally obtained that highly restrict their subsequent poling under very high voltage (>500 kV/cm).[3,16,18,25] Another alternative lies on the use of the poly(vinylidene fluoride-*co*-trifluoroethylene) copolymers, that is, P(VDF-*co*-TrFE), that could directly develop the ferroelectric and piezoelectric crystal phase either from the melt state or from solvent casting.[2] Despite interesting ferroelectric performances with remanent polarizations up to 11 μC/cm^2, the use of P(VDF-*co*-TrFE) copolymers still faces several limitations. These copolymers display a ferroelectric−paraelectric crystal transition at temperature down to 50−70 °C (depending on the TrFE content) that could restrict high-temperature applications. The cost of such copolymer is also very restrictive for their large-scale applications using melt-state processes of the plastic industry and solvent-based processing methods such as spin coating are preferred. In this context, new approaches are required to reach high β-phase content using neat PVDF by environmental-friendly and cost-effective processes, in particular thin film extrusion processing.

Melt-blending PVDF with a miscible polymer was also found to promote PVDF crystallization into the β-phase from the melt-state due to specific interactions between PVDF and a (partially) miscible polymer. This is the case of poly(methyl methacrylate) (PMMA) with the occurrence of dipole−dipole interactions between electrical moments of the carbonyl groups of PMMA and of the CF_2 groups of PVDF. Specific H-bonding interactions between the carbonyl oxygens of PMMA and CH_2 groups of PVDF with reduced strength due to conformational disorder cannot be totally excluded in these PVDF/PMMA blends.[26] Abundant literature regarding PVDF/PMMA miscibility, β-phase crystallization induced by PMMA and ferroelectric behavior for PVDF/PMMA blends[12,27−35] has already been reported. Briefly, using a solvent-based approach, Domenici et al. also demonstrated that the incorporation of 30 wt % of PMMA totally promotes the β-phase to the detriment of α-phase.[31] Leonard et al. also specifically observed that the PVDF crystallization is sensitive to the cooling rate applied from the melt state,[32] and according to these observations, a recent investigation was performed by our group using flash differential scanning calorimetry (FDSC) to identify the impact of the cooling rate from the melt state on the crystallization of neat PVDF and PVDF/PMMA blends.[33,36] These thermal analyses under fast cooling rates allowed us to obtain quantitative information on the crystallization temperature of nonpolar and polar phases over a large range of cooling rates (−10 to −4000 °C/s). A high cooling rate plays an essential role on the appearance of the PVDF β-phase with a clear α-to-β crystal transition. The polar β-phase starts to crystallize for cooling rates higher than 400 °C/s for neat PVDF with an exclusive, full crystallization for cooling rates beyond 1000−2000 °C/s. PMMA significantly shifted the α-to-β transition to lower cooling rates with the polar β-phase crystallization starting at cooling rates close to 50−100 °C/s with 10 wt % PMMA.[33] These results allowed us to obtain a clear crystal phase diagram of α-to-β crystal transition (with α+β mixed crystallization regime) as a function of PMMA and cooling rate. These diagrams also revealed the ability of PVDF/PMMA blends to promote the polar β-phase with standard processing tools used in the plastic industry and the extrusion-calendering processing of PVDF/PMMA blends with an intense cooling rate applied during film calendering turned out to be an efficient way to produce thin films containing high amounts of β-crystals with only 5 wt % of PMMA.[33] This process coupled to the addition of PMMA consequently represents an effective approach to reach electroactive properties for PVDF using a cost-competitive melt-state technique without any solvent required and without supplementary pre- or post-processing treatments.

In terms of piezoelectric and ferroelectric properties, such PVDF/PMMA blends have not been deeply investigated, and the data from literature shows some discrepancies. Some authors reported reduced piezoelectric and ferroelectric properties such as remanent polarization (P_r) and coercive field (E_c) with the incorporation of PMMA into PVDF.[15,27] Recent results from our group also demonstrated a remanent polarization close to 2.4 μC/cm^2 with 10 wt % PMMA[33] at a poling field of 2000 kV/cm, much weaker than the value for stretched PVDF film (close to 5.5 μC/cm^2 at the same poling field[37]). PVDF crystal size effects could explain the reduction of the electroactive properties for PVDF/PMMA blends.[38] Other research groups investigated the role of amorphous/crystalline interphase in miscible PVDF/PMMA and showed significant importance of this interphase on the dielectric behavior.[19] Stingelin et al. observed complex ferroelectric behavior for PVDF/PMMA blends with a typical hysteresis loop related to a capacitance phenomenon in the case of PVDF/PMMA blends with 10 wt % PMMA.[27] The capacitance phenomenon seems to indicate charge trapping during high-voltage poling. This phenomenon could be linked to the crystal−amorphous interphase and the intercrystalline amorphous region with a swelling effect induced by PMMA on the crystalline component.[39] These investigations clearly indicate complex dielectric effects in PVDF/PMMA blends, and the effect of PMMA on ferroelectric and piezoelectric properties of PVDF requires careful examination to optimize PVDF/PMMA blends, in particular for melt-extruded films with a high amount of β-phase.

The inner structure and resultant physical properties of PVDF/PMMA blends could be modified and tailored using functional PMMA-based additives. Such approaches were previously depicted by several research group with block-like copolymers based on methyl methacrylate (MMA) and functional comonomers. Wang et al. reported the use of 1-vinyl-3-ethyl imidazolium bromine ionic liquids (IL) to prepare P(MMA-IL), which is incorporated into PVDF by solution mixing.[40] The imidazolium cation of the IL through

https://dx.doi.org/10.1021/acsapm.0c00351
ACS Appl. Polym. Mater. 2020, 2, 3766−3780

its ion−dipolar interactions with $-CF_2$ groups of PVDF can promote the PVDF β-phase and improve electric charge transfer in both amorphous and interphase regions. Poly(ethylene oxide)-*block*-poly(methyl methacrylate) (PEO-*b*-PMMA) or poly(methyl methacrylate-*co*-poly(ethylene glycol) methacrylate) (PMMA-*co*-PEGMA) mixed with PVDF could also exhibit higher ionic conductivity at room temperature ($(2.8-3) \times 10^{-3}$ S/m in comparison to 0.5×10^{-3} S/m for the neat PVDF).[41,42] Other block-like copolymers were studied to modify the electroactive PVDF properties such as zwitterionic blocks or poly(2-vinylpyridine), but no piezoelectric or ferroelectric measurements were shown.[43,44] It could also be noticed that peculiar relaxor or antiferroelectric-like properties were also depicted for PVDF-based materials blends with several copolymers (P(VDF-TrFE-CTFE)-*g*-PMMA, P(VDF-TrFE-CTFE)-*g*-PEMA, P(VDF-TrFE-CTFE)-*g*-PS; CTFE = chlorotrifluorethylene; PEMA = poly(ethyl methacrylate); PS = polystyrene) with interesting perspectives for energy storage or as supercapacitors.[45−47] In this context, the use of functional PMMA-based copolymers clearly represents an interesting approach to develop new PVDF/PMMA materials with enhanced physical properties, and a specific examination is mandatory.

In this respect, the following study is dedicated to the development of new PVDF materials using functional PMMA-based additives for the development of cost-effective advanced materials made by standard tools of the plastic industry. The incorporation of PMMA into PVDF combined with an extrusion-calendering technology was previously found of high interest for this purpose. An optimal PMMA content was detected close to 5 wt % but only modest ferroelectric properties were reached in agreement with a moderate β-crystal production during the extrusion-calendering process. In this context, we here propose to investigate the use of poly(methyl methacrylate-*co*-methacrylic acid) copolymers (PMMA-*co*-MAA, hereafter called PMMA-MAA) containing ionizable groups via the methacrylic acid moiety. This copolymer is theoretically able to modify the miscibility with PVDF, boost the β-crystal production during extrusion-calendering, and increase the resultant ferro- and piezoelectric performances. Such additives containing ionizable moieties could also modify the dielectric behavior of the blends with potential intense effects on ferro- and piezoelectric properties. Consequently, this study particularly emphasizes how the use of PMMA-MAA copolymers alter the PVDF/PMMA miscibility, the related β-phase crystallization during melt-state processing, and subsequent ferro- and piezoelectric properties. Based on a previous investigation by our group, a preliminary study was conducted by FDSC to identify the impact of PMMA-MAA on the β-phase crystallization. A transposition to extrusion-calendered films was then performed followed by wide angle X-ray scattering (WAXS)/Fourier transform infrared spectroscopy (FTIR) characterizations to detect and quantify crystalline phases. A particular interest was subsequently focused on the ferroelectric and piezoelectric performances of as-produced PVDF/PMMA-MAA blends. The occurrence of crystal transformations during high-voltage poling and the impact of the high-voltage poling temperature on ferroelectric performance of PVDF/PMMA blends are finally discussed.

2. EXPERIMENTAL SECTION

2.1. Materials. Poly(vinylidene difluoride) was kindly supplied by Arkema, France (hereafter called PVDF, grade Kynar 720, M_w 200 000 g·mol^{-1}, MVR 10 cm^3/10 min @ 230 °C, 5 kg). Poly(methyl methacrylate) was supplied by Evonik, Germany (hereafter called PMMA, grade 8N, M_w 97 000 g·mol^{-1}, MVR 3 cm^3/10 min @ 230 °C, 3.8 kg). Poly(methyl methacrylate-*co*-methacrylic acid) (hearafter called PMMA-MAA, M_w 34 500 g·mol^{-1}, MAA content 1.6 mol %) was supplied by Sigma-Aldrich Chemistry. Throughout this contribution, all percentages are given as weight percentage (wt %).

2.2. Processing of PVDF/PMMA and PVDF/PMMA-MAA Blends. PVDF-based blends with PMMA-based additives were melt-processed by a film extrusion-calendering process as described in a previous article by our group.[33] In a first step, PVDF and PMMA or PMMA-MAA were melt-blended in a corotating twin-screw extruder (Haake Rheomex PTW 16 OS, ThermoScientific, Germany) with a screw diameter of 16 mm for a L/D ratio of 40. Predetermined weight ratio of PVDF and PMMA or PMMA-MAA pellets was dry-blended, extruded (screw speed between 150 and 200 rpm, mass flow rate between 1 and 1.2 kg/h), and pelletized. Extrusion temperatures were set to 210 °C (except for the temperature of extrusion die set at 170 °C). As-produced blends were reprocessed by film extrusion-calendering with a Haake single-screw extruder with a L/D ratio equal to 16, a temperature profile of 170−210−210−230 °C (from the hopper to the die), and a screw speed of 60 rpm. A specific slit die for film extrusion (width 150 mm, thickness 800 μm) was used, and the film extrudate was subsequently calendered to obtain 20−40 μm thick films (accurately measured using a Köfer mechanical comparator, resolution ±1 μm). The calendering system is equipped with a cooling system using cold water (10 °C) within the cylinders (estimated cooling rate ±200 °C/s according to the literature).[33]

2.3. Characterizations. *2.3.1. Attenuated Total Reflectance Fourier Transform Infrared Spectroscopy (ATR-FTIR).* As-produced thin films were analyzed by attenuated total reflectance Fourier transform infrared spectroscopy (ATR-FTIR) using a BIO-RAD Excalibur spectrometer equipped with an ATR Harrick Split Pea apparatus from SAFIR Cie. Spectra were recorded using a spectral width ranging from 700 to 1400 cm^{-1} with a resolution of 4 cm^{-1} and an accumulation of 64 scans. Peak areas at selected wavenumbers were determined using local baselines. ATR-FTIR spectra were systematically normalized to a reference peak (872 cm^{-1}) to dismiss the impact of film thickness variations on IR absorbance.

PVDF α- and β-crystallinities in as-produced films by extrusion-calendering were evaluated by ATR-FTIR according to previous studies by Gregorio et al.[2,48] Relationships between peak intensity and crystal concentration were adapted for ATR-FTIR. The content in α-crystals was first calculated from relation 1 using baseline-corrected absorbance at 760 cm^{-1} (A_{760}) and at 870 cm^{-1} (A_{870}). The proportionality constant, $K_{760/840}$, was set to 1.4 using a reference PVDF sample fully crystallized into the α-phase ($X_{c\text{-}\alpha}$ 55% determined by DSC with an infinite ΔH_α of 104.5 J/g,[2,36,39] $A_{760}/A_{870} \approx 0.8$ determined by ATR-FTIR). The content in β-crystals was calculated from relation 2 using the baseline-corrected absorbance at 840 cm^{-1} (A_{840}). Since no reference PVDF sample fully crystallized into β-phase is available (with unknown value for infinite ΔH_β), the proportionality constant $K_{760/840}$ was obtained by relation 3 based on previous studies by Gregorio et al.[2,48]

$$X_{c\text{-}\alpha} = K_{760/870}^{\text{ATR-FTIR}} \frac{A_{760}}{A_{870}} \quad (1)$$

$$X_{c\text{-}\beta} = K_{840/870}^{\text{ATR-FTIR}} \frac{A_{840}}{A_{870}} \quad (2)$$

$$K_{840/870}^{\text{ATR-FTIR}} = 1.26 K_{760/870}^{\text{ATR-FTIR}} \quad (3)$$

2.3.2. 2D Small and Wide Angle X-ray Scattering (2D-SAXS and 2D-WAXS). As-produced thin films were analyzed by both small and wide angle X-ray scattering (SAXS and WAXS). Analyses were carried out at room temperature in transmission mode on a Xeuss apparatus

https://dx.doi.org/10.1021/acsapm.0c00351
ACS Appl. Polym. Mater. 2020, 2, 3766−3780

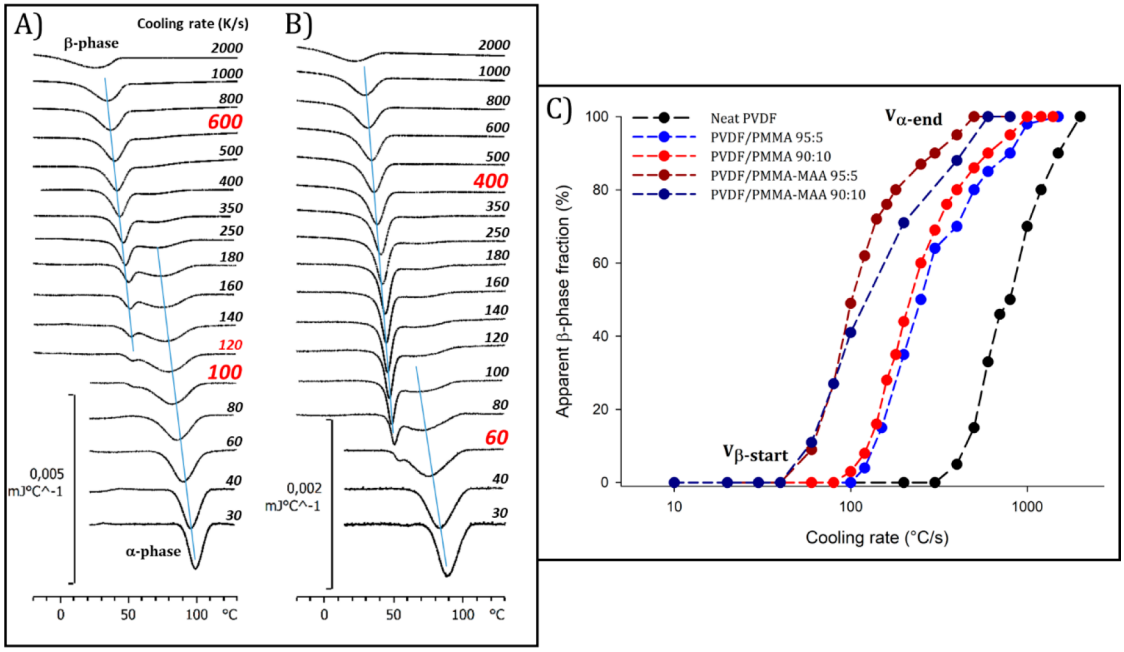

Figure 1. FDSC cooling scans at various cooling rates obtained for PVDF/PMMA-MAA blends with 5 wt % PMMA-MAA (A) and 10 wt % PMMA-MAA (B) (critical cooling rates for the appearance of the β-phase and disappearance of the α-phase are marked in red. Apparent β-phase fraction (C) as a function of the cooling rate for neat PVDF (black), PVDF/PMMA with 5 wt % PMMA (blue), PVDF/PMMA with 10 wt % PMMA (dark blue), PVDF/PMMA-MAA blends with 5 wt % PMMA-MAA (red) and PVDF/PMMA-MAA blends with 10 wt % PMMA-MAA (dark red). Data for neat PVDF and PVDF/PMMA with 5−10 wt % PMMA are taken from previous measurements.[33]

(Xenocs, France). Cu Kα radiation (λ = 1.542 Å) was used. The sample to detector distances (calibrated using silver behenate) were set to approximately 10 and 120 cm for WAXS and SAXS, respectively. The 2D patterns were recorded using a Pilatus detector (Dectris). Standard corrections (background, dark, etc.) were applied to the patterns before analyses, and integrated intensity profiles were computed using the Foxtrot software.

2.3.3. DSC and Flash DSC (FDSC). Flash DSC (FDSC) experiments were carried out on a Mettler-Toledo Flash DSC 1 via a specific protocol to observe the crystallization behavior of as-produced PVDF/PMMA-based blends at different cooling rates. The detailed procedure can be found in our previous article on this topic.[33] Briefly, samples of about 35−100 ng were placed on the active area of the circular 500 μm diameter sensor using an optical microscope. The FDSC method for crystallization analyses is the following: heating at 1000 °C/s to 210 °C, isotherm at 210 °C during 10 s, cooling at controlled cooling rates between −10 °C/s and −4000 °C/s to −80 °C, isotherm at −80 °C during 10 s, heating at 5000 °C/s to 210 °C. Crystallization temperatures (T_c) were determined at the maximum of the exothermic peak observed during the cooling scan. For the sake of clarity, cooling curves were normalized by the cooling rate.

2.3.4. Ferroelectric and Piezoelectric Properties. All electrical characterizations were carried out on metallized thin films with Ag electrodes deposited by vacuum sputtering (electrode area 7 mm^2). Ferroelectric-type $P-E$ and $I-E$ loops were characterized in a dielectric liquid bath (FC40, 3MTM FluorinertTM) by a current integration method.[49−51] Low-frequency (0.1 Hz) and high-voltage sine waves were applied by the combination of a synthesizer/function generator (HP3325B, Hewlett-Packard Inc., Palo Alto, CA) and a high-voltage amplifier (Trek model 10/40A, Medina, NY). Surface charges were measured with a homemade charge-to-voltage converter. Ferroelectric-type $P-E$ and $I-E$ loops are presented after compensation, that is, after subtracting linear polarization and conduction contributions from the current response, by assuming a resistance and a capacitance in a parallel model. For each measurement (i.e., for each applied electric field), several consecutive high-voltage cycles (3−5 cycles) were performed to ensure a stable switching behavior. The piezoelectric coefficient d_{33} was then obtained with a Berlincourt piezometer (Channel Products Inc. Chesterland, OH, mechanical stress condition of 100 Hz and 0.25 N). High-voltage poling was accomplished under the maximum field attained during $P-E$ and $I-E$ characterizations (typically 1500 kV/cm) by removing the field just before completing the loop. The Ag electrodes were eventually removed for specific physicochemical analysis using cotton tips impregnated with diluted hydrochloric acid followed by immediate rising with distilled water.

2.3.5. Visual and Optical Inspections. Optical properties of as-produced thin films (transmittance, haze, and clarity) were investigated and quantified using a specific test bench from BKY Gardner (Germany, HazeGrad Plus). As-produced thin films were also investigated by optical microscopy in reflection mode using Leica DM 2500 M microscope (magnification ×20) to reveal blend microstructures.

3. RESULTS AND DISCUSSION

3.1. PVDF/PMMA-MAA Miscibility and β-Phase Crystallization Analyzed by FDSC. To get precise information regarding the PVDF/PMMA-MAA miscibility and the use of PMMA-MAA as a β-phase promoter for PVDF, a preliminary study was conducted by flash DSC on selected compositions before a transposition to extrusion-calendered films. PVDF blends with 5−10 wt % PMMA-MAA obtained using a melt-state twin-screw extrusion process were submitted to FDSC analysis and crystallization exotherms from the melt state were recorded at various cooling rates, ranging from 10 to 2000 °C/s (Figure 1A,B). Particular attention was paid to the α-to-β crystal transition with respect to the cooling rate (Figure 1C), and the apparent β-phase fraction as a function of the cooling rate was extracted from relative crystallization enthalpies. Comparisons with PVDF/PMMA blends were performed, and crystallization temperatures T_c were also extracted for α/β-

https://dx.doi.org/10.1021/acsapm.0c00351
ACS Appl. Polym. Mater. 2020, 2, 3766−3780

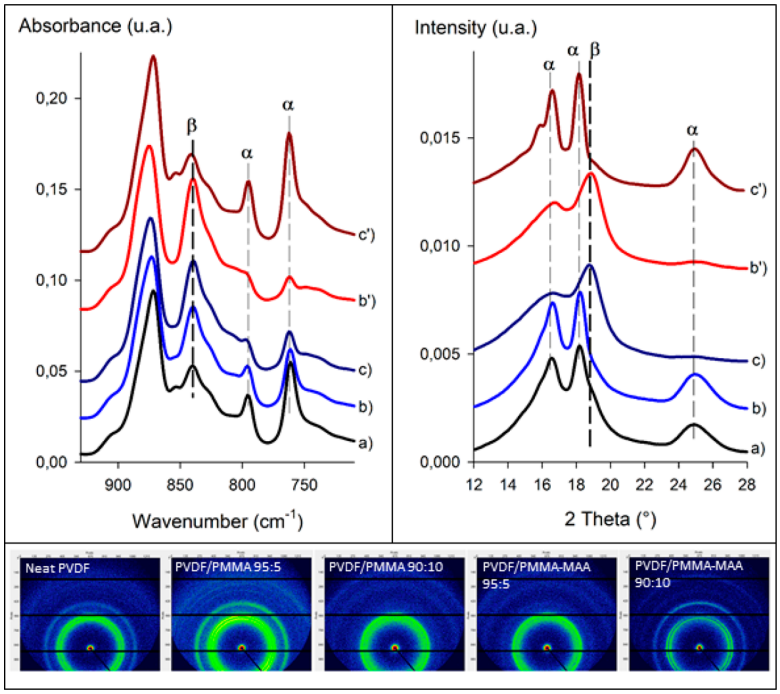

Figure 2. ATR-FTIR (left) and WAXS (right) spectra of PVDF/PMMA and PVDF/PMMA-MAA blends processed into films by extrusion-calendering. Neat PVDF (a, black), PVDF/PMMA 95:5 (b, blue), PVDF/PMMA-MAA 95:5 (c, dark blue), PVDF/PMMA 90:10 (b′, red), and PVDF/PMMA-MAA 90:10 (c′, dark red). Corresponding 2D-WAXS spectra are displayed in the lower box.

crystallizations (Figure S1) to get a better view of PVDF/PMMA-MAA miscibility.

PVDF/PMMA-MAA blends with 5 wt % PMMA-MAA exhibit a single exotherm for low cooling rates (<100 °C/s) with crystallization temperatures in the range of 110−70 °C. A second distinct exotherm at lower crystallization temperatures in the range 60−20 °C appears at higher cooling rates and becomes predominant at elevated cooling rates. Based on previous studies by our group,[33] the first exotherm is ascribed to the PVDF α-crystallization and the second low-temperature exotherm to the PVDF β-crystallization. Thus, the PMMA-MAA copolymer also was prone to the α-to-β crystal transition, similarly to neat PVDF and PVDF/PMMA blends (at 5 wt % PMMA). The α-to-β crystal transition occurs between 100 and 600 °C/s, such values being much lower than neat PVDF with β-phase crystallization starting around 400 °C/s.[33] The evolution of the crystallization temperatures as a function of the cooling rate (Figure S1) also reveals a significant shift to lower T_c for both α- and β-crystallization in PVDF/PMMA-MAA compared to neat PVDF attesting to good PVDF/PMMA-MAA miscibility. A comparison could be also performed with the corresponding PVDF/PMMA blend with 5 wt % PMMA. The efficiency of PMMA-MAA for β-phase production seems to be slightly better than PMMA with a tiny reduction of the crystallization temperatures and shift of α-to-β crystal transition (transition in the range 120−700 °C/s for PVDF/PMMA blend with 5 wt % PMMA) (Figure S1).

For PVDF/PMMA-MAA blends with 10 wt % PMMA-MAA, the α-to-β crystal transition is clearly shifted to lower cooling rates in a similar way to that of PVDF/PMMA blends.[33] The β-phase could appear for cooling rates as low as 60 °C/s and slightly better performances are again observed for PVDF/PMMA-MAA containing 10 wt % PMMA-MAA compared to PMMA (in particular at elevated cooling rates). Significant reductions of the α-/β-crystallization temperatures are also detected (Figure S1). In this context, FDSC consequently suggests good miscibility of PMMA-MAA with PVDF in the concentration range 5−10 wt % PMMA-MAA with slight positive influence of PMMA-MAA compared to PMMA for the β-phase production during cooling from the melt state (in particular at representative cooling rate of the extrusion-calendering process). These effects could be attributed to enhanced PVDF/PMMA-MAA interactions inducing higher miscibility with PVDF, in agreement with findings by Landis et al. on PVDF crystallization in the presence of tiny amounts of PMMA-MAA.[52]

3.2. β-Phase Crystallization in PVDF/PMMA-MAA Films Produced by Extrusion-Calendering. Taking into account FDSC results, thin films of PVDF/PMMA-MAA (thickness range of 25−35 μm) were produced by melt-state extrusion-calendering process that provide intense cooling rates (±200 °C/s depending on film thickness and materials).[33] Thin films were then characterized by ATR-FTIR and WAXS to observe the evolution of the PVDF crystalline phases with the incorporation of 5 and 10 wt % PMMA-MAA. ATR-FTIR is an accurate characterization technique for PVDF crystalline phases that potentially enables qualitative and quantitative measurements for the β-phase (characteristic absorption peak at 840 cm^{-1}) and for the α-phase (characteristic absorption peak at 766, 795, and 855 cm^{-1}).[2,48,53] To discriminate the polar phases and confirm ATR-FTIR analyses, WAXS characterizations were used to identify the crystalline lattices[2] related to β- and α-phase at a 2θ angle of 20.8° and 18.3°, 19.9°, and 26.6°, respectively. ATR-FTIR and WAXS analyses are also useful to detect the PVDF γ-phase (characteristic absorption peaks at 776, 812, and 1234 cm^{-1}).[2,48,53] Figure 2 displays ATR-FTIR and WAXS characterizations of PVDF, PVDF/PMMA, and PVDF/

https://dx.doi.org/10.1021/acsapm.0c00351
ACS Appl. Polym. Mater. 2020, 2, 3766−3780

PMMA-MAA blends. First, the neat PVDF film displays mostly the characteristic peaks of the nonpolar α-phase (765, 795, and 855 cm^{-1}). A slight β-phase crystallization is observed (840 cm^{-1}) due to high cooling rates. WAXS analysis for neat PVDF films also shows the apparition of a small shoulder at 20.5°, which confirms the small amount of β-phase.

For PVDF/PMMA and PVDF/PMMA-MAA blends with 5 wt % PMMA-based additives, a clear modification of the PVDF crystallization is observed. ATR-FTIR allows confirmation of the high positive influence of PMMA-MAA on the β-phase crystallization during film extrusion-calendering compared to that from PMMA. Indeed, the absorption peak related to the β-phase at 840 cm^{-1} clearly displays higher intensity for the PVDF/PMMA-MAA blend than the corresponding PVDF/PMMA blend. In contrast, α-phase absorption peaks are reduced. WAXS analysis confirms the effect of PMMA-MAA on β-phase crystallization with a clear β-phase pattern (20.3°) and a quasi-disappearance of the α-phase diffraction peak at 2θ angle close to 26.6°. To complete these analysis, it could be mentioned that (i) ATR-FTIR/WAXS characterizations are unable to detect significant amounts of PVDF γ-phase (absence of absorption peaks at 776 and 812 cm^{-1}, unclear assignment of the absorption peak at 1240 cm^{-1}, Figure S2) thus confirming the α-to-β crystal transition in PVDF/PMMA blends processed by extrusion-calendering (with a possible occurrence of a small PVDF γ-phase fraction) and (ii) unoriented α/β-crystals are detected by 2D-WAXS (Figure 2) indicating that α/β-crystallization seems to proceed from a quasi-isotropic melt state. In this context, PMMA-MAA acts as a powerful β-phase promoter for PVDF using a melt-state extrusion-calendering process, such result being partly consistent with previous FDSC experiments. Actually, it could be stated that the efficiency of PMMA-MAA seems to be significantly higher in dynamic conditions (i.e., after shearing treatments by extrusion) than in static conditions (i.e., during FDSC analysis).

Similar analyses were performed for PVDF-based blends with 10 wt % PMMA-based additives (Figure 2), and ATR-FTIR/WAXS experiments clearly show an opposite evolution in terms of PVDF crystallization. First, the incorporation of 10 wt % PMMA favors β-crystallization as observed by the increase of β-peak intensity and the typical WAXS patterns of β-phase, in accordance with previous studies.[33] In contrast, the incorporation of 10 wt % PMMA-MAA drastically inhibited the β-phase crystallization. A predominant α-phase and a very low β-phase content is detected for this particular blend, such result being confirmed by WAXS analysis. Deeper investigations were performed to detect the miscibility extent after the extrusion process of this particular blend using visual/optical inspections and SAXS analysis (Figure S3). The PVDF/PMMA-MAA blend with 10 wt % PMMA-MAA displays an opaque appearance that was quantified by optical measurements with a higher haze value (21% compared to 4−5% for other blends) coupled to a lower clarity value (77% compared to 99−97% for other blends). This effect is linked to the heterogeneous, texturized microstructure of this particular blend and suggests a reduced miscibility extent. The peculiar 2D-SAXS pattern also confirmed the presence of nanoscale oriented/elongated domains. All these elements coupled to the significant discrepancy with previous FDSC analysis clearly suggest that PVDF/PMMA-MAA blends are unstable in dynamic/shearing conditions. This demixing phenomenon in shearing conditions induces complex effects on PVDF crystallization (enhanced β-phase crystallization at 5 wt % PMMA-MAA and inhibited β-phase crystallization at 10 wt % PMMA-MAA). Such conclusions could agree with previous conclusions from Landis et al. demonstrating that an elevated quantity of MAA moieties could have a negative effect on the resulting compatibility.[52] Finally, differences in molecular weight between PMMA-MAA (37 500 g/mol) and PMMA (97 000 g/mol) with large subsequent differences in melt viscosity and terminal relaxation times could explain this demixing phenomena in intense shear/elongation flows. Detailled investigations are required in the future to reproduce this phenomenon in a controlled shear/elongation environment to stabilize and control the microstructure and the miscibility extent of PVDF/PMMA-MAA blends (in particular at elevated PMMA-MAA content.

Quantitative information about PVDF α- and β-crystallinities in as-produced thin films were obtained by ATR-FTIR, and the evolution of PVDF crystal contents with the amount of PMMA or PMMA-MAA is tabulated in Table 1. Neat PVDF films display a total crystallinity of ±56% ($\alpha+\beta$ crystals) with approximately 45−50% α-crystals and 5−10% β-crystals. The evolution of PVDF total crystallinity as a function of PMMA content displays a continuous decrease in agreement with the PVDF/PMMA miscibility.[28,33] In addition, the content in α-crystals clearly and quickly drops with the amount of PMMA with a total disappearance for 20 wt %, in agreement with the α-to-β crystal transition with the incorporation of PMMA. The amount of β-phase reaches the entire crystallinity at this particular PMMA content. Similar calculations were performed for PVDF/PMMA-MAA with an interesting β-phase content of 35% (total crystallinity 45%, β-phase fraction 78%, Table 1) for only 5 wt % PMMA-MAA. The high reduction of the β-phase content in PVDF/PMMA-MAA blends incorporating high PMMA-MAA loadings (10 wt %) is here confirmed (total crystallinity 52%, β-phase content 8%). To conclude, compared to the use of PMMA, PMMA-MAA clearly enhances the production of PVDF β-crystals from the melt state using an extrusion-calendering process with elevated cooling rates applied to thin films. However, the amount of PMMA-MMA should be carefully controlled and limited to 5 wt % to avoid demixing phenomena in dynamic shearing conditions during extrusion at higher PMMA-MAA loadings.

Table 1. PVDF Crystalline Phase Contents in PVDF/PMMA and PVDF/PMMA-MAA Blends Processed into Films Produced by Extrusion-Calendering[a]

	$X_{c\text{-}\alpha\text{-crystals}}$ (%)	$X_{c\text{-}\beta\text{-crystals}}$ (%)	$X_{c\text{-}\alpha+\beta\text{-crystals}}$ (%)
neat PVDF	48(4)	8(4)	56(1)
PVDF/PMMA 95:5	33(4)	19(4)	52(1)
PVDF/PMMA 90:10	16(2)	27(2)	43(1)
PVDF/PMMA 80:20	1(1)	31(1)	32(1)
PVDF/PMMA-MAA 95:5	10(1)	35(1)	45(1)
PVDF/PMMA-MAA 90:10	43(2)	8(1)	52(1)

[a]α-Crystals, β-crystals, and total $\alpha+\beta$-crystals; evaluation by ATR-FTIR, standard deviation given in parentheses.

3.3. Ferroelectric Properties of PVDF/PMMA-MAA Films Produced by Extrusion-Calendering. Previous crystallinity characterizations enable selection of interesting materials for subsequent ferroelectric and piezoelectric studies. Actually, the PVDF/PMMA-MAA blend displays an interest-

https://dx.doi.org/10.1021/acsapm.0c00351
ACS Appl. Polym. Mater. 2020, 2, 3766−3780

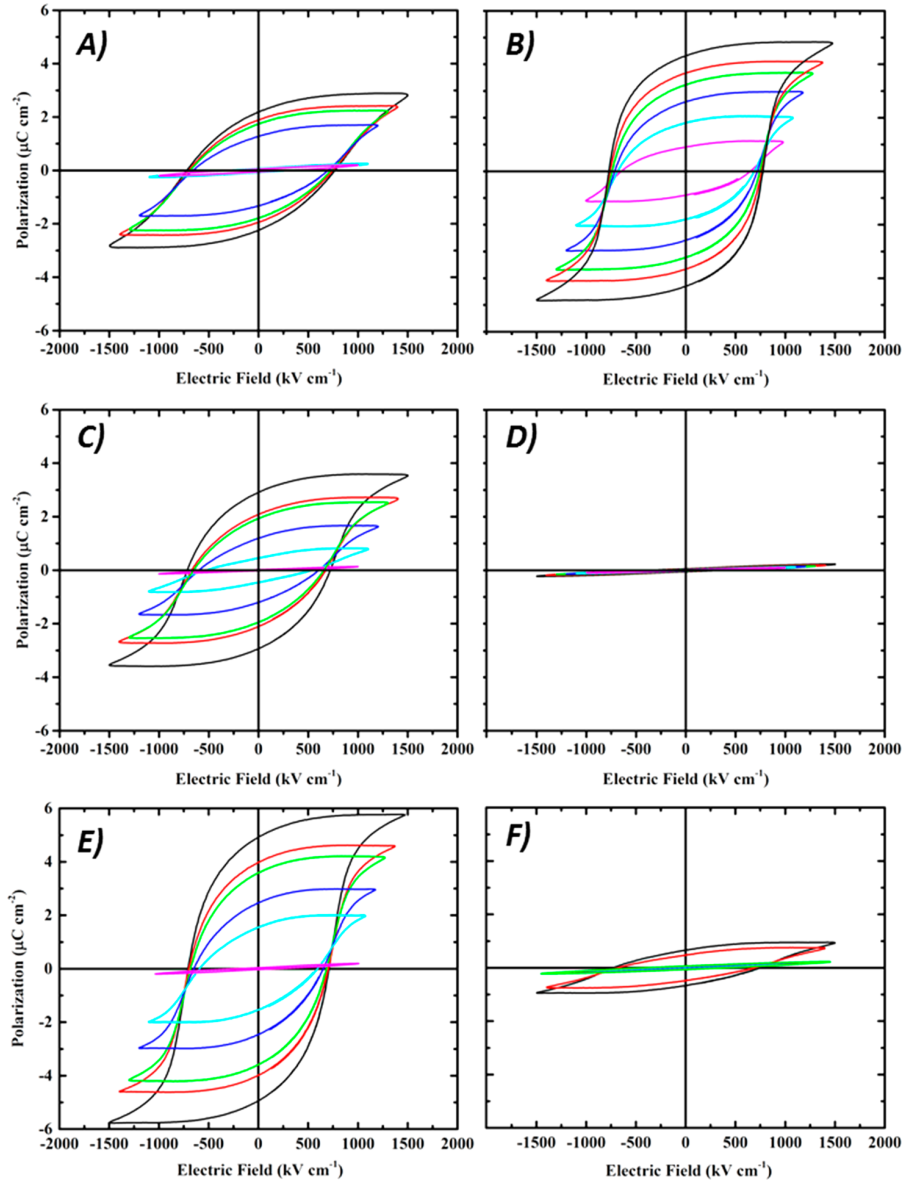

Figure 3. *P*−*E* hysteresis loops under increasing AC electric fields recorded at room temperature for PVDF/PMMA and PVDF/PMMA-MAA blends processed into films by extrusion-calendering. Neat PVDF (A), PVDF/PMMA 95:5 (B), PVDF/PMMA 90:10 (C), PVDF/PMMA 80:20 (D), PVDF/PMMA-MAA 95:5 (E) and PVDF/PMMA-MAA 90:10 (F) (film thickness 25−35 μm).

ing β-phase content of 35% (total crystallinity 45%, β-phase fraction 78%) with only 5 wt % PMMA-MAA and thus represents an interesting candidate for ferro- and piezoelectric applications. To analyze ferroelectric properties and performance under poling at high AC electric fields and obtain correlations to PVDF crystal structures, *P*−*E* and *I*−*E* hysteresis loops were recorded for as-produced thin films by extrusion-calendering. These loops allow the identification and quantification of the ferroelectric switching behavior with the ability to perform an efficient poling under AC electric fields for further piezoelectric testing. The remanent polarization, P_r (permanent dipole orientation or polarization after voltage removal), is extracted from the *P*−*E* loops along with a ferroelectric quality factor (i.e., ratio between remanent polarization and saturation polarization, P_r/P_{sat}, with P_{sat} being the maximum dipole orientation or polarization achieved for each applied voltage). *I*−*E* loops reveal charge displacements inside the analyzed materials with the estimation of the coercive field, E_c (electric field required for dipole switching). Figure 3 displays *P*−*E* loops from neat PVDF, PVDF/PMMA, and PVDF/PMMA-MAA films at various electric fields ranging from 1000 to 1500 kV/cm. Corresponding *I*−*E* loops can be found in the Supporting Information, Figure S4. Quantitative values for P_r and E_c at the maximal electric field of 1500 kV/cm are tabulated in Table 2, and Figure 4 gathers the evolution of P_r and E_c values as a function of the electric field.

With an applied electric field of 1500 kV/cm, neat PVDF displays ferroelectric-type behavior (Figure 3A) with P_r close to 2.2 μC/cm^2, E_c close to 825 kV/cm, and a quality factor of 0.78 (Table 2). These values are lower than those obtained by Mackey et al.[37] on stretched PVDF poled at the same electric field (P_r close to 5.5 μC/cm^2). Discrepancies are also observed

https://dx.doi.org/10.1021/acsapm.0c00351
ACS Appl. Polym. Mater. 2020, 2, 3766−3780

Table 2. Remanent Polarization, Coercive Field and Ferroelectric Quality Factor for PVDF/PMMA and PVDF/PMMA-MAA Blends Processed into Films by Extrusion-Calendering[a]

	P_r (μC/cm^2)	E_c (kV/cm)	P_r/P_{sat}
neat PVDF	2.2	825	0.78
PVDF/PMMA 95:5	4.3	770	0.88
PVDF/PMMA 90:10	3.0	760	0.79
PVDF/PMMA 80:20	0.1	*b*	0.22
PVDF/PMMA-MAA 95:5	4.9	740	0.85
PVDF/PMMA-MAA 90:10	0.6	*b*	*b*

[a]AC electric field 1500 kV/cm; film thickness 25−35 μm. [b]Not measured.

with previously reported results in the corresponding literature,[8,33,37,54,55] partly attributed to (i) the impact of the extrusion processing method with high cooling rates to produce polar β-crystals and (ii) compensation procedures to remove nonswitching charges during $P-E$ and $I-E$ measurements. It should be noted that neat PVDF showed a hard ferroelectric switching behavior for electric fields below 1200 kV/cm with back-switching phenomena (dipole rotation without full switch or fixation).[56] It is also clear from $P-E$ loops that neat PVDF is far from polarization saturation and thus higher electric fields than 1500 kV/cm would be required. $I-E$ curves also indicate that the switching is not homogeneous throughout the material with a broad distribution of coercive fields typically observed with poorly poled materials in the preswitching regime (Figure S4).

Incorporating 5 wt % PMMA into PVDF clearly improves ferroelectric properties (Figure 3B) with P_r up to 4.3 μC/cm^2, E_c close to 770 kV/cm, and a quality factor of 0.88 at the maximal electric field of 1500 kV/cm (Table 2). These values still remain below those reported for stretched PVDF poled at the same electric field, but square $P-E$ loops approaching polarization saturation are obtained, and $I-E$ curves indicate a more homogeneous switching behavior with a narrower distribution of coercive fields (Figure S4). However, higher PMMA content (10 wt %) clearly reduces ferroelectric properties with a total transformation into quasi-linear dielectric-like behavior at 20 wt % PMMA (Figure 3C,D and Table 2), despite a continuous increase of polar β-phase content with higher amounts of PMMA (β-phase content up to 31% at 20 wt % PMMA, β-phase fraction close to 100% Table 1). This apparent ferroelectric vanishing could be related to a strong clamping of β-phase dipoles that hinders their effective polarization. This is a well-known phenomenon in ferroelectric materials usually associated with the presence of dipolar defects that interact with the spontaneous polarization.

The addition of 5 wt % PMMA-MAA copolymer into PVDF further improved ferroelectric properties in comparison with the corresponding PVDF/PMMA blend (Figure 3E). P_r close to 5 μC/cm^2, E_c of 740 kV/cm, and an excellent quality factor of 0.85 are obtained at the maximal electric field of 1500 kV/cm (Table 2). Again, square $P-E$ loops indicate that polarization saturation is being approached with homogeneous switching behavior (Figure S4). Coercive fields are interestingly lower in PVDF/PMMA-MAA (with higher remanent polarization), and these effects indicate that the PMMA-MAA copolymer modifies not only the dipole density (related to β-phase content) but also its own switching dynamics. Higher incorporation of PMMA-MAA again results in reduced ferroelectric properties, but in this case, this effect is in agreement with the significant decrease of β-phase content for 10 wt % PMMA-MAA related to its immiscibility with PVDF (Figure 3F and Table 2).

Figure 4 gives an interesting overview and allows conclusions about the evolution of the ferroelectric properties with the applied electric field and the type and amount of PMMA additives. Neat PVDF needs elevated electric fields (>1200 kV/cm) to induce ferroelectric switching behavior with high E_c values. With the addition of 5 wt % PMMA or PMMA-MAA, ferroelectric-type behaviors appear at lower electric fields with significant increase of the remanent polarizations, lower coercive fields, and higher ferroelectric quality factors. These results are evidence that ferroelectric PVDF-based films could be produced by a melt-state extrusion-calendering process. The specific use of 5 wt % PVDF/PMMA-MAA clearly enhanced ferroelectric properties. Such effect is primarily attributed to the improvement of the β-phase content induced by the extrusion-calendering processing (β-phase content up to 35%), but a contribution of ionic moieties to the dipole dynamics is also suspected. Our results also evidence that the initial β-phase content does not seem to fully govern the final ferroelectric behavior and properties. Actually, neat PVDF with a low β-phase content displays small but interesting ferroelectric properties, and no clear correla-

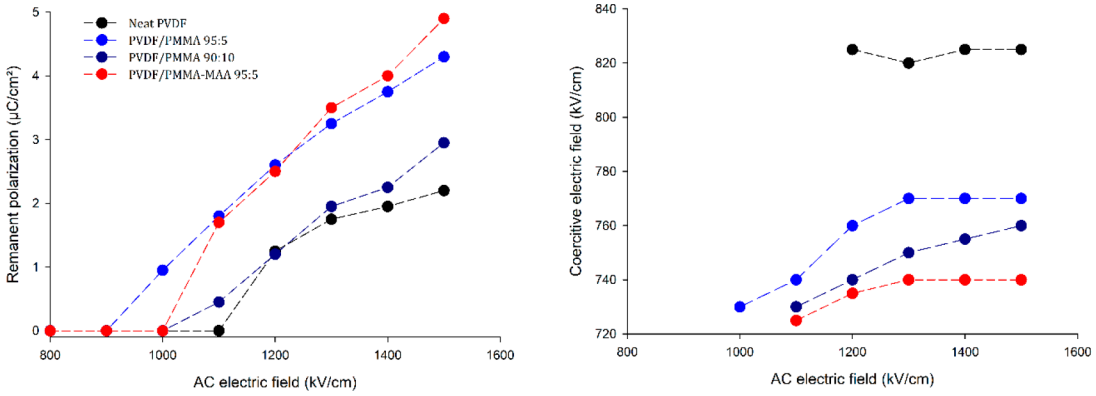

Figure 4. Evolution of the remanent polarization (left) and coercive electric field (right) with the applied AC electric field for neat PVDF (black), PVDF/PMMA 95:5 (blue), PVFD/PMMA 90:10 (dark blue), and PVDF/PMMA-MAA 95:5 (red) blends processed into films by extrusion-calendering (film thickness 25−35 μm).

https://dx.doi.org/10.1021/acsapm.0c00351
ACS Appl. Polym. Mater. 2020, 2, 3766−3780

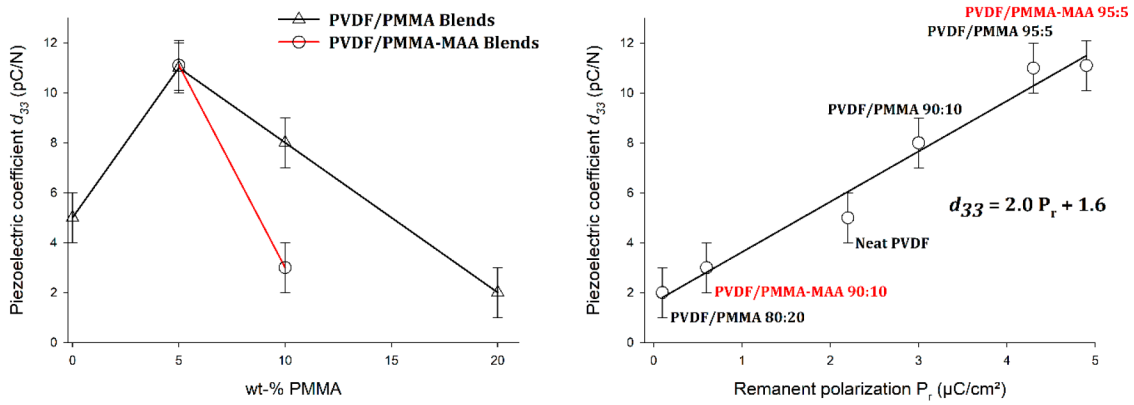

Figure 5. Evolution of the piezoelectric coefficient d_{33} with the amount of PMMA-based additives (left) and evolution of the piezoelectric coefficient d_{33} with the remanent polarization (right) for PVDF/PMMA and PVDF/PMMA-MAA blends processed into films by extrusion-calendering (high-voltage poling by AC electric field 1500 kV/cm, film thickness 25−35 μm).

tions are found between the remanent polarization achieved at elevated electric fields and the initial β-phase content. Other factors or parameters probably need to be considered for an in-depth understanding (like crystalline modifications at elevated electric fields, the size of PVDF β-crystals, and interfacial trapped charges[33]). However, a partial α-to-β crystal phase transformation under high electric fields is particularly anticipated in as-produced blends, and this effect will be discussed within the next sections.

3.4. Piezoelectric Properties of PVDF/PMMA-MAA Films Produced by Extrusion-Calendering. Ferroelectric properties of PVDF-based materials are known to be correlated with their final piezoelectric properties, and such properties are clearly of high interest for many emerging applications. The corresponding literature indicates that ferroelectric and piezoelectric properties can be significantly affected by the presence of PMMA,[15,27] and taking into account previous results on ferroelectric properties, piezoelectric coefficients, d_{33}, were evaluated for as-produced PVDF/PMMA-MAA blends. The time stability of the piezoelectric coefficients d_{33} up to 2 weeks after the poling process was first addressed, and quantitative values can be found in the Supporting Information, Table S1. The piezoelectric coefficient of neat PVDF after the poling procedure was found to be close to 7 pC/N (±1 pC/N) decreasing to a stabilized value of 5 pC/N after a storage period of 1 week (Table S1). Thus, a first remarkable result is that as-produced neat PVDF film displays a significant d_{33} value without stretching treatments.[1−4] PVDF/PMMA blends with 5, 10, and 20 wt % PMMA additives were subsequently subjected to the same poling procedure followed by piezoelectric measurements (Table S1). As a general rule, the piezoelectric coefficient also decreases with storage time by approximately 1−2 pC/N after 1 week to reach a stabilized value. Such effects could be linked to residual electrostatic charges (electret effect) or charge losses inside the matrices due to relaxations. However, it could be stated that stable piezoelectric properties are obtained for as-produced and as-poled PVDF/PMMA blends.

Figure 5 displays the evolution of the piezoelectric coefficient as a function of the PMMA or PMMA-MAA content. The evolution of the piezoelectric coefficient closely follows the trend observed in ferroelectric properties. Actually, a maximal d_{33} value is observed with 5 wt % PMMA or PMMA-MAA reaching a remarkable piezoelectric coefficient of approximately 11 pC/N. For higher PMMA or PMMA-MAA contents, piezoelectric properties drastically decrease. A close correlation is anticipated between piezoelectric coefficients (d_{33}) and remanent polarizations (P_r), and as depicted in Figure 5, a linear relationship between d_{33} and P_r is nearly obtained with a slope of approximately 2. Such linear relationship is clearly in agreement with recent models concerning the piezoelectricity of PVDF, in particular with the electrostriction model[57] that yields a linear relationship with a slope close to 2.4. It could be noticed that the line does not pass through the origin with a residual piezoelectricity of approximately 1.5 pC/N as confirmed with PVDF/PMMA blends incorporating high PMMA contents up to 20 wt %. These effects could be ascribed to trapped charges introduced during poling into as-produced PVDF/PMMA. As a conclusion, interesting piezoelectric properties are observed for PVDF blends with PMMA and PMMA-MAA processed into films by an extrusion-calendering technique. The impact of PMMA or PMMA-MAA on the piezoelectric properties is obvious with a maximal coefficient close to 11 pC/N for an optimum content of 5 wt %. Nevertheless, in this case, no significant differences are noticed between PVDF/PMMA and PVDF/PMMA-MAA blends in terms of piezoelectric activity. An interesting correlation with a linear relationship is obtained between piezoelectric and ferroelectric properties in PVDF/PMMA and PVDF/PMMA-MAA blends that points out the main importance of ferroelectric properties for further optimization.

3.5. Discussion on Crystal Transformations during High-Voltage Poling. As previously discussed, the initial β-phase content in as-produced PVDF-based films does not fully fit with ferroelectric properties and subsequent piezoelectric properties. Actually, neat PVDF films with a poor β-phase content develop significant ferro- and piezoelectric properties, but several PVDF/PMMA blends (in particular, PVDF/PMMA blends with 10−20 wt % PMMA) with high β-phase contents display poor ferro- and piezoelectric performances. An optimal content close to 5 wt % is required to boost ferro- and piezoelectric properties, but despite significant differences between PVDF/PMMA and PVDF/PMMA-MAA blends in terms of initial β-phase content, similar P_r and, in particular, d_{33} values are obtained. One potential and interesting hypothesis lies in crystal transformations during high-voltage poling with a potential α-to-β crystal transformation at elevated electric

https://dx.doi.org/10.1021/acsapm.0c00351
ACS Appl. Polym. Mater. 2020, 2, 3766−3780

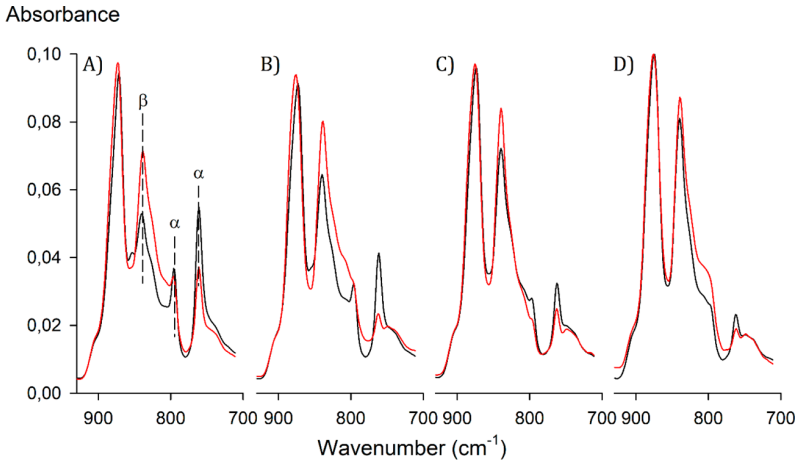

Figure 6. Impact of high-voltage poling on the ATR-FTIR spectra of neat PVDF (A), PVDF/PMMA 95:5 (B), PVDF/PMMA 90:10 (C), and PVDF/PMMA-MAA 95:5 (D) blends processed into films by extrusion-calendering (AC electric field 1500 kV/cm, film thickness 25−35 μm). Poled (red) and nonpoled (black).

fields.[58,59] Such modifications could drastically modify ferroelectric properties with repercussions on subsequent piezoelectric performances.

In this context, additional ATR-FTIR experiments were conducted on the PVDF−PMMA and PVDF/PMMA-MAA films processed by extrusion-calendering after the high-voltage poling process at 1500 kV/cm. ATR-FTIR spectra were compared with previous results before high-voltage poling (Figure 6), and quantitative parameters regarding crystal type/content are tabulated in Table 3. Based on ATR-FTIR spectra,

Table 3. PVDF Crystalline Phase Contents in Poled PVDF/PMMA and PVDF/PMMA-MAA Blends Processed into Films by Extrusion-Calendering[a]

	$X_{c\text{-}\alpha\text{-crystals}}$ (%)	$X_{c\text{-}\beta\text{-crystals}}$ (%)	$X_{c\text{-}\alpha+\beta\text{-crystals}}$ (%)
neat PVDF	20 (−28)	29 (+21)	49 (−7)
PVDF/PMMA 95:5	8 (−25)	38 (+19)	45 (−7)
PVDF/PMMA 90:10	6 (−10)	33 (+6)	40 (−3)
PVDF/PMMA 80:20	1 (0)	31 (0)	32 (0)
PVDF/PMMA-MAA 95:5	5 (−5)	39 (+4)	44 (−1)
PVDF/PMMA-MAA 90:10	44 (0)	10 (+1)	53 (+1)

[a] α-Crystals, β-crystals, and $\alpha+\beta$-crystals; evaluation by ATR-FTIR, AC electric field 1500 kV/cm, film thickness 25−35 μm, variations compared to unpoled films given in parentheses.

crystalline modifications clearly occurred in neat PVDF films during high-voltage poling with a high increase in polar β-phase content from 8% to 29% (Figure 6A and Table 3). The α-phase content also clearly decreases in a similar magnitude, thus confirming an α-to-β crystal transformation during high-voltage poling for neat PVDF films and explaining the sizable ferroelectric switching behavior observed for this material.

Similar final crystal transformations are observed for PVDF/PMMA and PVDF/PMMA-MAA with 5 wt % PMMA or PMMA-MAA with an increase of the β-phase peaks after poling together with a decrease of α-phase peaks (Figure 6B,C). The final amount of β-crystals reaches 38−39% for these blends (Table 3) in accordance with their enhanced ferroelectric properties. However, ferroelectric properties cannot be entirely correlated to the final amount of β-crystals after high-voltage poling, in particular for PVDF/PMMA blends with 20 wt % PMMA (β-phase content close to 31%, β-phase fraction close to 100%). Actually, the α-to-β crystal transformation is known to occur via an intermediate polar α-phase, named α_p-phase, leading to a global α-to-α_p-to-β crystal transformation under high-voltage poling.[58,59] This pathway is here difficult to detect using ATR-FTIR, but several abnormal trends are detected. On one hand, Table 3 highlights variations in terms of total crystalline content before and after high-voltage poling with an apparent decrease in total crystallinity. In addition, the α-crystal peak located at 795 cm^{-1} corresponding to $-CH_2$ rocking vibrations[60] seems to follow different trends from the other α-crystal, and this absorption peak does not decrease after high-voltage poling. In this context, a (partial) crystal transformation from the α-phase into α_p-phase during high-voltage poling seems consistent with our observations. Consequently, thanks to α-to-α_p-to-β crystal transformation during poling, it can be assumed that a high initial β-phase content is not fully mandatory for enhanced ferro- and piezoelectric performances. The nonpolar α-phase could also contribute to ferroelectric properties of neat PVDF and PVDF/PMMA blends via a polar intermediate α_p-phase. The amount of these two crystalline phases after high poling voltage seems to control ferroelectric properties of PVDF/PMMA and PVDF/PMMA-MAA blends processed by extrusion-calendering. In-depth and challenging investigations are required in the near future to detect exact mechanisms behind α-to-α_p-to-β crystal transformation and the exact role of each crystalline phase (and *in fine* the role of PMMA and PMMA-MAA copolymers) on ferroelectric and piezoelectric properties of PVDF/PMMA and PVDF/PMMA-MAA blends.

3.6. High-Voltage Poling at Elevated Temperatures of PVDF−PMMA Blends. Previous results demonstrate (i) the importance of P_r on piezoelectric coefficients d_{33} and (ii) the occurrence of crystal transformations during the high-voltage AC poling (controlling the final β/α_p-phase contents and the resulting P_r). The use of PMMA-MAA also induces higher ferroelectric properties, and the presence of ionizable moieties is also expected to modify the dielectric behavior of the resulting blend, in particular at elevated temperatures where ionic conduction mechanisms could be activated. In this respect, high-voltage AC poling experiments were carried out

https://dx.doi.org/10.1021/acsapm.0c00351
ACS Appl. Polym. Mater. 2020, 2, 3766−3780

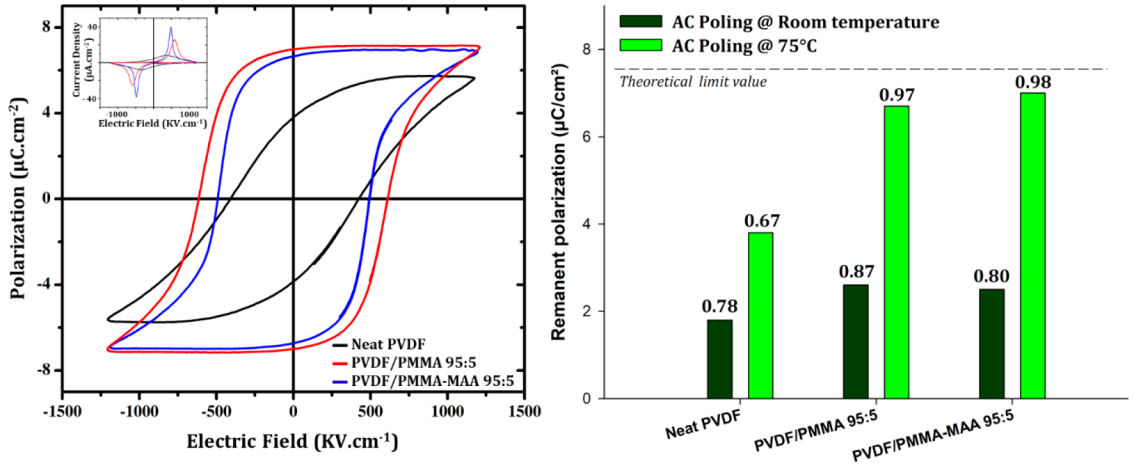

Figure 7. *P*−*E* loops recorded at 75 °C for neat PVDF (black), PVDF/PMMA 95:5 (blue), and PVDF/PMMA-MAA 95:5 (red) blends processed into films by extrusion-calendering (left). Corresponding *I*−*E* curves in the inset. Subsequent impact of poling temperature on remanent polarization of as-produced films (AC electrical field 1200 kV/cm, film thickness 25−35 μm, ferroelectric quality factor P_r/P_{sat} above bars) (right).

at elevated temperatures (75 °C) to boost ferroelectric properties via the specific use of PMMA-MAA. *P*−*E* and *I*−*E* hysteresis loops at 75 °C for neat PVDF, PVDF/PMMA, and PVDF/PMMA-MAA blends (5 wt % additives) are displayed in Figure 7. Quantitative information (P_r, E_c and ferroelectric quality factors) are given in the Supporting Information, Table S2.

High-voltage poling at 75 °C significantly enhances the ferroelectric switching behavior of PVDF/PMMA and PVDF/PMMA-MAA blends, and very high remanent polarizations close to 6.7 and 7.0 μC/cm^2 were achieved, respectively (Table S2). PVDF/PMMA and PVDF/PMMA-MAA display similar ferroelectric properties, but slightly better performances are obtained with PMMA-MAA. Both materials show square *P*−*E* loops with nearly saturated polarization and ferroelectric quality factors close to 1 indicating the absence of dipole relaxation. *I*−*E* curves also indicate fairly homogeneous dipole switching. The high-quality ferroelectric loops with large P_r and low E_c are quite similar to recent studies on PVDF-TrFE films poled under similar conditions.[57] Interestingly, ab initio studies indicate a maximal spontaneous polarization of about 18.8 μC/cm^2 for PVDF β-crystals.[61,62] Considering the maximum amount of β-phase achieved after high-voltage poling (close to 40%), the maximal remanent polarization attainable would be about 7.5 μC/cm^2 in our materials (which can be enhanced to about 8.5 μC/cm^2 in the case of full α-to-α_p-to-β crystal conversion with a final β-phase content of 45%). In this context, the high-voltage poling process at elevated temperature clearly enables a nearly perfect poling of β-crystals in PVDF/PMMA-MAA to reach high P_r values close to the theoretical limit value. Potential piezoelectric coefficients up to 16 pC/N are expected (according to Figure 5).

Neat PVDF also shows the same positive trend regarding the impact of the poling temperature on the ferroelectric switching behavior, and remanent polarizations up to 3.8 μC/cm^2 were achieved at 75 °C (Table S2). However, *P*−*E* loops are still far from polarization saturation with a reduced ferroelectric quality factor, and *I*−*E* curves indicate inhomogeneous switching with a very broad distribution of coercive fields. Such effects are in accordance with an enhanced amorphous phase mobility inducing a reduced dipole coupling due to dipole relaxation within the amorphous phase.[63,64] In this respect, the use of PMMA and in particular PMMA-MAA is clearly crucial to enable a nearly perfect poling of β-crystals at elevated poling temperature with high P_r values and to produce high-quality ferroelectric behaviors.

The origin of such high-quality ferroelectric behaviors obtained at elevated poling temperature still remain complex to identify, but PMMA and PMMA-MAA are suspected to activate particular ionic conduction mechanisms inside the amorphous phase that enhance and stabilize charge compensation effects or modify the effective internal electric field. Such modifications of the ionic conductivity have been already detected in PVDF/PMMA blends with an increase of the electrical conductivity from approximately (0.8 to 200) × 10^{-15} S/cm between 23 and 90 °C respectively (compared to (5−700) × 10^{-15} S/cm in the case of neat PVDF).[65] Such conclusions are also in agreement with the ionic nature of PMMA-MAA that naturally brings new conduction mechanisms, in particular at elevated temperature.

In conclusion, high-voltage AC poling at elevated temperatures clearly represents an interesting approach to boost ferroelectric and piezoelectric performances of melt-processed PVDF-based blends using functional PMMA-MAA additives in low amounts. The use of PMMA-MAA (and even PMMA) is clearly crucial to enable a nearly perfect poling of β-crystals at elevated poling temperature and to produce high-quality ferroelectric behaviors with high P_r values up to the theoretical limit value. Several hypotheses need to be tested in the near future, in particular (i) the impact of the high-voltage poling temperature on the α-to-α_p-to-β crystal transformation, (ii) the role of the electrical conductivity on charge compensation, trapping, and stabilization (in PVDF/PMMA blends), and (iii) the role of dipole relaxation within the amorphous phase. The time−temperature stability of ferroelectric and piezoelectric behavior induced by high-voltage poling at elevated temperatures also need further investigations for practical applications.

4. CONCLUSIONS

PVDF/PMMA-MAA blends were processed into thin films by an industrially relevant melt-state extrusion-calendering, and several characterizations were conducted to identify the role of PMMA-MAA on β-phase crystallization and subsequent ferro-

https://dx.doi.org/10.1021/acsapm.0c00351
ACS Appl. Polym. Mater. 2020, 2, 3766−3780

and piezoelectric properties. FDSC experiments highlight good miscibility between PVDF and PMMA-MAA. The PMMA-MAA copolymer acts as a PVDF β-phase promoter with a slightly better efficiency than PMMA (slight shift of α-to-β crystal transition toward lower cooling rates compared to the corresponding blends with PMMA). A transposition to melt-processed PVDF-based blends by extrusion-calendering was attempted, and ATR-FTIR/WAXS analysis attested to intensive production of the PVDF β-phase in PVDF/PMMA-MAA with a specific incorporation of 5 wt % PMMA-MAA. In this respect, thin films based on PVDF/PMMA-MAA with high amounts of polar crystals (β-phase fraction up to 80%, β-phase crystallinity up to 35%) could be produced by an industrially relevant melt extrusion-calendering process, and this blend seems to be a promising ferroelectric and piezoelectric material. However, the amount of PMMA-MAA should be limited to 5 wt % due demixing phenomena at higher PMMA-MAA loadings. Discrepancies are observed with FDSC analysis that indicate peculiar effects of the extrusion-calendering processing (shearing or pressure-induced demixing) on the β-phase crystallization.

Ferroelectric properties at room temperature were established for PVDF/PMMA-MAA blends processed by extrusion-calendering using $P-E$ and $I-E$ hysteresis loops. The best performances are observed with the incorporation of 5 wt % PMMA-MAA with a P_r value up to 4.9 $\mu C/cm^2$ using a AC electric field of 1500 kV/cm (value close to stretched PVDF). This effect seems to arise from the enhanced β-phase content for this specific formulation. Piezoelectric properties were also improved at an optimal content of 5 wt % PMMA or PMMA-MAA with a maximal value close to 11 pC/N. A clear linear relationship between P_r and d_{33} has been demonstrated confirming the importance of ferroelectric properties to optimize piezoelectric properties of PVDF/PMMA blends. Despite higher initial β-phase content in PVDF/PMMA-MAA, only modest improvements were noticed for PVDF/PMMA-MAA blends compared to PVDF/PMMA blends.

Finally, a complex crystal transformation occurs during high-voltage poling, in accordance with an α-to-α_p-to-β crystal transformation pathway. A maximal amount of β-phase close to 38−39% is obtained with the specific use of 5 wt % PMMA or PMMA-MAA. The role of the α_p-phase is indirectly evidenced, in particular for neat PVDF. Finally, high-voltage poling at elevated temperatures (up to 75 °C) could significantly improve ferroelectric performance and quality of the PVDF/PMMA-MAA blend (P_r values up to 7.0 $\mu C/cm^2$). PVDF/PMMA blend also shows interesting (but lower) ferroelectric properties, which demonstrates the crucial role of PMMA-MAA combined with high-voltage poling at elevated temperatures. This copolymer clearly enabled a nearly perfect poling of β-crystals at elevated poling temperature to produce high-quality ferroelectric behaviors with high P_r values up to the theoretical limit value (and with theoretical piezoelectric coefficients d_{33} up to 16 pC/N). Underlying phenomena still require in-depth investigations in the near future on various scientific and technical aspects (impact of the shearing on the α-to-β crystal crystallization, precise α-to-α_p-to-β crystal transformation pathway, role of the electrical conductivity and dipole relaxation within the amorphous phase on charge trapping and stabilization, time−temperature stability of ferroelectric and piezoelectric performances). However, this study clearly demonstrates that PVDF blends with miscible functional PMMA copolymers such as PMMA-MAA consequently represent an interesting approach to develop cost-effective electroactive polymer materials for advanced ferro- and piezoelectric devices using industrially relevant processes.

■ ASSOCIATED CONTENT

Supporting Information

The following files are available free of charge. File type PDF. The Supporting Information is available free of charge at https://pubs.acs.org/doi/10.1021/acsapm.0c00351.

Crystallization temperatures for α- and β-crystals detected by FDSC as a function of the cooling rate for neat PVDF, PVDF/PMMA with 5 wt % PMMA, PVDF/PMMA with 10 wt % PMMA, PVDF/PMMA-MAA blends with 5 wt % PMMA-MAA, and PVDF/PMMA-MAA blends with 10 wt % PMMA-MAA, full ATR-FTIR spectra of PVDF/PMMA and PVDF/PMMA-MAA blends processed into films by extrusion-calendering, optical inspections of PVDF/PMMA and PVDF/PMMA-MAA blends processed into films by extrusion-calendering and corresponding 2D-SAXS spectra, $I-E$ hysteresis loops under increasing AC electric fields for PVDF/PMMA and PVDF/PMMA-MAA blends processed into films by extrusion-calendering, time stability of the piezoelectric coefficient d_{33} for PVDF/PMMA and PVDF/PMMA-MAA blends processed into films by extrusion-calendering, and remanent polarization and coercive electric field as a function of the high-voltage poling temperature for PVDF-based blends with PMMA and PMMA-MAA processed into films by extrusion-calendering (PDF)

■ AUTHOR INFORMATION

Corresponding Author

Cédric Samuel − *Ecole Nationale Supérieure Mines Telecom Lille Douai, Institut Mines Telecom Lille Douai (IMT Lille Douai), Département Technologie des Polymères et Composites & Ingénierie Mécanique (TPCIM), Cité Scientifique, F-59650 Villeneuve-d'Ascq, France;* orcid.org/0000-0003-0101-4992; Email: cedric.samuel@imt-lille-douai.fr

Authors

Alexandre De Neef − *University of Mons (UMons), Laboratory of Polymeric and Composite Materials (LPCM), Center of Innovation and Research in Materials and Polymers (CIRMAP), B-7000 Mons, Belgium; Ecole Nationale Supérieure Mines Telecom Lille Douai, Institut Mines Telecom Lille Douai (IMT Lille Douai), Département Technologie des Polymères et Composites & Ingénierie Mécanique (TPCIM), Cité Scientifique, F-59650 Villeneuve-d'Ascq, France*

Harvey Amorín − *Instituto de Ciencia de Materiales de Madrid (ICMM), Consejo Superior de Investigaciones Científicas (CSIC), 28049 Madrid, Spain;* orcid.org/0000-0001-9915-1631

Gregory Stoclet − *Université de Lille, CNRS, INRAE, Centrale Lille, UMR 8207 − UMET − Unité Matériaux et Transformations (UMET), F-59000 Lille, France*

Ricardo Jiménez − *Instituto de Ciencia de Materiales de Madrid (ICMM), Consejo Superior de Investigaciones Científicas (CSIC), 28049 Madrid, Spain*

Philippe Dubois − *University of Mons (UMons), Laboratory of Polymeric and Composite Materials (LPCM), Center of*

https://dx.doi.org/10.1021/acsapm.0c00351
ACS Appl. Polym. Mater. 2020, 2, 3766−3780

Innovation and Research in Materials and Polymers (CIRMAP), B-7000 Mons, Belgium

Jérémie Soulestin − *Ecole Nationale Supérieure Mines Telecom Lille Douai, Institut Mines Telecom Lille Douai (IMT Lille Douai), Département Technologie des Polymères et Composites & Ingénierie Mécanique (TPCIM), Cité Scientifique, F-59650 Villeneuve-d'Ascq, France*

Jean-Marie Raquez − *University of Mons (UMons), Laboratory of Polymeric and Composite Materials (LPCM), Center of Innovation and Research in Materials and Polymers (CIRMAP), B-7000 Mons, Belgium;* orcid.org/0000-0003-1940-7129

Complete contact information is available at: https://pubs.acs.org/10.1021/acsapm.0c00351

Author Contributions

The manuscript was written through contributions of all authors. All authors have given approval to the final version of the manuscript. All authors contributed equally.

Notes

The authors declare no competing financial interest.

■ ACKNOWLEDGMENTS

Authors gratefully acknowledge the Wallonia Region/Service Public de Wallonie (Belgium), West Vlaanderen Region (Belgium), Agentschap Innoveren Ondernemen (Belgium) and European Commission (FEDER) for the financial support in the framework of the INTERREG V FWVL program (BIOHARV project, GoToS3 portofolio). Authors particularly thank Samuel Devisme from Arkema (France) for supplying raw materials. UMons (LPCM) gratefully acknowledges the Belgian Federal Government Office of Science Policy/Belgian Federal Science Policy Office (SSTC − PAI 6/27, Belgium) for general support and is much indebted to both the Wallonia Region/Service Public de Wallonie (Belgium) and the European Commission (FEDER) for financial support in the frame of phasing-out Hainaut. IMT Lille Douai and Université de Lille acknowledge both the International Campus on Safety and Intermodality in Transportation (CISIT, France), the Hauts-de-France Region (France) and the European Commission (FEDER) for their contributions to funding extrusion equipment, SAXS-WAXS laboratory equipment and calorimetric characterization tools. Authors also thank the Spanish Ministerio de Economía y Competitividad (MINECO) for financial supports of MAT2017-88788-R and MAT2016-76851-R projects.

■ REFERENCES

(1) Ameduri, B. From Vinylidene Fluoride (VDF) to the Applications of VDF-Containing Polymers and Copolymers: Recent Developments and Future Trends. *Chem. Rev.* **2009**, *109* (12), 6632−6686.

(2) Martins, P.; Lopes, A. C.; Lanceros-Mendez, S. Electroactive Phases of Poly(Vinylidene Fluoride): Determination, Processing and Applications. *Prog. Polym. Sci.* **2014**, *39* (4), 683−706.

(3) Murayama, N.; Nakamura, K.; Obara, H.; Segawa, M. The Strong Piezoelectricity in Polyvinylidene Fluroide (PVDF). *Ultrasonics* **1976**, *14* (1), 15−24.

(4) Kepler, R. G.; Anderson, R. A. Ferroelectricity in Polyvinylidene Fluoride. *J. Appl. Phys.* **1978**, *49* (3), 1232−1235.

(5) Stadlober, B.; Zirkl, M.; Irimia-Vladu, M. Route towards Sustainable Smart Sensors: Ferroelectric Polyvinylidene Fluoride-Based Materials and Their Integration in Flexible Electronics. *Chem. Soc. Rev.* **2019**, *48* (6), 1787−1825.

(6) Vatansever, D.; Hadimani, R. L.; Shah, T.; Siores, E. An Investigation of Energy Harvesting from Renewable Sources with PVDF and PZT. *Smart Mater. Struct.* **2011**, *20* (5), 055019.

(7) Shepelin, N. A.; Glushenkov, A. M.; Lussini, V. C.; Fox, P. J.; Dicinoski, G. W.; Shapter, J. G.; Ellis, A. V. New Developments in Composites, Copolymer Technologies and Processing Techniques for Flexible Fluoropolymer Piezoelectric Generators for Efficient Energy Harvesting. *Energy Environ. Sci.* **2019**, *12* (4), 1143−1176.

(8) Zhu, L. Exploring Strategies for High Dielectric Constant and Low Loss Polymer Dielectrics. *J. Phys. Chem. Lett.* **2014**, *5* (21), 3677−3687.

(9) Zhu, L.; Wang, Q. Novel Ferroelectric Polymers for High Energy Density and Low Loss Dielectrics. *Macromolecules* **2012**, *45* (7), 2937−2954.

(10) Jones, R. E.; Maniar, P. D.; Moazzami, R.; Zurcher, P.; Witowski, J. Z.; Lii, Y. T.; Chu, P.; Gillespie, S. J. Ferroelectric Non-Volatile Memories for Low-Voltage, Low-Power Applications. *Thin Solid Films* **1995**, *270* (1−2), 584−588.

(11) Das, S.; Appenzeller, J. FETRAM. An Organic Ferroelectric Material Based Novel Random Access Memory Cell. *Nano Lett.* **2011**, *11* (9), 4003−4007.

(12) Kang, S. J.; Park, Y. J.; Bae, I.; Kim, K. J.; Kim, H. C.; Bauer, S.; Thomas, E. L.; Park, C. Printable Ferroelectric PVDF/PMMA Blend Films with Ultralow Roughness for Low Voltage Non-Volatile Polymer Memory. *Adv. Funct. Mater.* **2009**, *19* (17), 2812−2818.

(13) Jeon, J. H.; Kang, S. P.; Lee, S.; Oh, I. K. Novel Biomimetic Actuator Based on SPEEK and PVDF. *Sens. Actuators, B* **2009**, *143* (1), 357−364.

(14) Mohammadi, B.; Yousefi, A. A.; Bellah, S. M. Effect of Tensile Strain Rate and Elongation on Crystalline Structure and Piezoelectric Properties of PVDF Thin Films. *Polym. Test.* **2007**, *26* (1), 42−50.

(15) Hahn, B. R.; Wendorff, J. H. Piezo- and Pyroelectricity in Polymer Blends of Poly(Vinylidene Fluoride)/Poly(Methyl Methacrylate). *Polymer* **1985**, *26* (11), 1611−1618.

(16) Bharti, V.; Kaura, T.; Nath, R. Ferroelectric Hysteresis in Simultaneously Stretched and Corona-Poled PVDF Films. *IEEE Trans. Dielectr. Electr. Insul.* **1997**, *4* (6), 738−741.

(17) Gomes, J.; Nunes, J. S.; Sencadas, V.; Lanceros-Mendez, S. Influence of the β-Phase Content and Degree of Crystallinity on the Piezo- and Ferroelectric Properties of Poly(Vinylidene Fluoride). *Smart Mater. Struct.* **2010**, *19* (6), No. 065010.

(18) Das-Gupta, D. K.; Doughty, K. Corona Charging and the Piezoelectric Effect in Polyvinylidene Fluoride. *J. Appl. Phys.* **1978**, *49* (8), 4601−4603.

(19) Hahn, B.; Wendorff, J.; Yoon, D. Y. Dielectric Relaxation of the Crystal-Amorphous Interphase in Poly(Vinylidene Fluoride) and Its Blends with Poly(Methyl Methacrylate). *Macromolecules* **1985**, *18* (4), 718−721.

(20) Hahn, B. R.; Herrmann-Schönherr, O.; Wendorff, J. H. Evidence for a Crystal-Amorphous Interphase in PVDF and PVDF/PMMA Blends. *Polymer* **1987**, *28* (2), 201−208.

(21) Martins, P.; Nunes, J. S.; Hungerford, G.; Miranda, D.; Ferreira, A.; Sencadas, V.; Lanceros-Méndez, S. Local Variation of the Dielectric Properties of Poly(Vinylidene Fluoride) during the α- to β-Phase Transformation. *Phys. Lett. A* **2009**, *373* (2), 177−180.

(22) Lund, A.; Gustafsson, C.; Bertilsson, H.; Rychwalski, R. W. Enhancement of β Phase Crystals Formation with the Use of Nanofillers in PVDF Films and Fibres. *Compos. Sci. Technol.* **2011**, *71* (2), 222−229.

(23) Mishra, S.; Kumaran, K. T.; Sivakumaran, R.; Pandian, S. P.; Kundu, S. Synthesis of PVDF/CNT and Their Functionalized Composites for Studying Their Electrical Properties to Analyze Their Applicability in Actuation & Sensing. *Colloids Surf., A* **2016**, *509*, 684−696.

(24) Ke, K.; Pötschke, P.; Jehnichen, D.; Fischer, D.; Voit, B. Achieving β-Phase Poly(Vinylidene Fluoride) from Melt Cooling:

Effect of Surface Functionalized Carbon Nanotubes. *Polymer* **2014**, *55* (2), 611−619.
(25) Sencadas, V.; Lanceros-Méndez, S.; Mano, J. F. Characterization of Poled and Non-Poled β-PVDF Films Using Thermal Analysis Techniques. *Thermochim. Acta* **2004**, *424* (1−2), 201−207.
(26) Léonard, C.; Halary, J. L.; Monnerie, L. Hydrogen Bonding in PMMA-Fluorinated Polymer Blends: FTi.r. Investigations Using Ester Model Molecules. *Polymer* **1985**, *26* (10), 1507−1513.
(27) Li, M.; Stingelin, N.; Michels, J. J.; Spijkman, M. J.; Asadi, K.; Feldman, K.; Blom, P. W. M.; De Leeuw, D. M. Ferroelectric Phase Diagram of PVDF:PMMA. *Macromolecules* **2012**, *45* (18), 7477−7485.
(28) Sasaki, H.; Kanti Bala, P.; Yoshida, H.; Ito, E. Miscibility of PVDF/PMMA Blends Examined by Crystallization Dynamics. *Polymer* **1995**, *36* (25), 4805−4810.
(29) Okabe, Y.; Murakami, H.; Osaka, N.; Saito, H.; Inoue, T. Morphology Development and Exclusion of Noncrystalline Polymer during Crystallization in PVDF/PMMA Blends. *Polymer* **2010**, *51* (6), 1494−1500.
(30) Linares, A.; Acosta, J. L. Tensile and Dynamic Mechanical Behaviour of Polymer Blends Based on PVDF. *Eur. Polym. J.* **1997**, *33* (4), 467−473.
(31) Domenici, C.; De Rossi, D.; Nannini, A.; Verni, R. Piezoelectric Properties and Dielectric Losses in PVDF-PMMA Blends. *Ferroelectrics* **1984**, *60* (1), 61−70.
(32) Léonard, C.; Halary, J. L.; Monnerie, L. Crystallization of Poly(Vinylidene Fluoride)-Poly(Methyl Methacrylate) Blends: Analysis of the Molecular Parameters Controlling the Nature of the Poly(Vinylidene Fluoride) Crystalline Phase. *Macromolecules* **1988**, *21* (10), 2988−2994.
(33) De Neef, A.; Samuel, C.; Stoclet, G.; Rguiti, M.; Courtois, C.; Dubois, P.; Soulestin, J.; Raquez, J. M. Processing of PVDF-Based Electroactive/Ferroelectric Films: Importance of PMMA and Cooling Rate from the Melt State on the Crystallization of PVDF Beta-Crystals. *Soft Matter* **2018**, *14* (22), 4591−4602.
(34) Wang, Y. D.; Cakmak, M. Hierarchical Structure Gradients Developed in Injection-molded PVDF and PVDF−PMMA Blends. I. Optical and Thermal Analysis. *J. Appl. Polym. Sci.* **1998**, *68* (6), 909−926.
(35) Zhao, X.; Chen, S.; Zhang, J.; Zhang, W.; Wang, X. Crystallization of PVDF in the PVDF/PMMA Blends Precipitated from Their Non-Solvents: Special Orientation Behavior, Morphology, and Thermal Properties. *J. Cryst. Growth* **2011**, *328* (1), 74−80.
(36) Gradys, A.; Sajkiewicz, P.; Adamovsky, S.; Minakov, A.; Schick, C. Crystallization of Poly(Vinylidene Fluoride) during Ultra-Fast Cooling. *Thermochim. Acta* **2007**, *461* (1−2), 153−157.
(37) Mackey, M.; Schuele, D. E.; Zhu, L.; Flandin, L.; Wolak, M. A.; Shirk, J. S.; Hiltner, A.; Baer, E. Reduction of Dielectric Hysteresis in Multilayered Films via Nanoconfinement. *Macromolecules* **2012**, *45* (4), 1954−1962.
(38) Yang, X.; Kong, X.; Tan, S.; Li, G.; Ling, W.; Zhou, E. Spatially-Confined Crystallization of Poly(Vinylidene Fluoride). *Polym. Int.* **2000**, *49* (11), 1525−1528.
(39) Oikonomou, E. K.; Tencé-Girault, S.; Gérard, P.; Norvez, S. Swelling of Semi-Crystalline PVDF by a PMMA-Based Nanostructured Diblock Copolymer: Morphology and Mechanical Properties. *Polymer* **2015**, *76*, 89−97.
(40) Wang, P.; Xu, P.; Zhou, Y.; Yang, Y.; Ding, Y. Effect of MWCNTs and P[MMA-IL] on the Crystallization and Dielectric Behavior of PVDF Composites. *Eur. Polym. J.* **2018**, *99*, 58−64.
(41) Xiao, Q.; Wang, X.; Li, W.; Li, Z.; Zhang, T.; Zhang, H. Macroporous Polymer Electrolytes Based on PVDF/PEO-b-PMMA Block Copolymer Blends for Rechargeable Lithium Ion Battery. *J. Membr. Sci.* **2009**, *334* (1−2), 117−122.
(42) Li, H.; Lin, C. E.; Shi, J. L.; Ma, X. T.; Zhu, B. K.; Zhu, L. P. Preparation and Characterization of Safety PVDF/P(MMA-Co-PEGMA) Active Separators by Studying the Liquid Electrolyte Distribution in This Kind of Membrane. *Electrochim. Acta* **2014**, *115*, 317−325.
(43) Tu, K.; Shen, P.; Li, J.; Fan, B.; Yang, C.; Du, R. Preparation of Enduringly Antifouling PVDF Membrane with Compatible Zwitterionic Copolymer via Thermally Induced Phase Separation. *J. Appl. Polym. Sci.* **2015**, *132* (7), 41362.
(44) Wang, L.; Chen, S. Crystallization Behaviors of Poly(Vinylidene Fluoride) and Poly(Methyl Methacrylate)-Block-Poly(2-Vinyl Pyridine) Block Copolymer Blends. *J. Therm. Anal. Calorim.* **2016**, *125* (1), 215−230.
(45) Gong, H.; Miao, B.; Zhang, X.; Lu, J.; Zhang, Z. High-Field Antiferroelectric-like Behavior in Uniaxially Stretched Poly(Vinylidene Fluoride-Trifluoroethylene-Chlorotrifluoroethylene)-Grafted-Poly(Methyl Methacrylate) Films with High Energy Density. *RSC Adv.* **2016**, *6* (2), 1589−1599.
(46) Li, J.; Gong, H.; Yang, Q.; Xie, Y.; Yang, L.; Zhang, Z. Linear-like Dielectric Behavior and Low Energy Loss Achieved in Poly(Ethyl Methacrylate) Modified Poly(Vinylidene-Co-Trifluoroethylene). *Appl. Phys. Lett.* **2014**, *104* (26), 263901.
(47) Guan, F.; Wang, J.; Yang, L.; Tseng, J. K.; Han, K.; Wang, Q.; Zhu, L. Confinement-Induced High-Field Antiferroelectric-like Behavior in a Poly(Vinylidene Fluoride-Co-Trifluoroethylene-Co-Chlorotrifluoroethylene)-Graft-Polystyrene Graft Copolymer. *Macromolecules* **2011**, *44* (7), 2190−2199.
(48) Gregorio, R.; Cestari, M. Effect of Crystallization Temperature on the Crystalline Phase Content and Morphology of Poly(Vinylidene Fluoride). *J. Polym. Sci., Part B: Polym. Phys.* **1994**, *32* (5), 859−870.
(49) Amorín, H.; Jiménez, R.; Deluca, M.; Ricote, J.; Hungría, T.; Castro, A.; Algueró, M. Nanostructuring Effects in Piezoelectric BiScO3 -PbTiO 3 Ceramics. *J. Am. Ceram. Soc.* **2014**, *97* (9), 2802−2809.
(50) Amorín, H.; Jiménez, R.; Ricote, J.; Hungría, T.; Castro, A.; Algueró, M. Apparent Vanishing of Ferroelectricity in Nanostructured $BiScO_3$-$PbTiO_3$. *J. Phys. D: Appl. Phys.* **2010**, *43* (28), 285401−285406.
(51) Qiu, X.; Holländer, L.; Wirges, W.; Gerhard, R.; Cury Basso, H. Direct Hysteresis Measurements on Ferroelectret Films by Means of a Modified Sawyer-Tower Circuit. *J. Appl. Phys.* **2013**, *113* (22), 224106.
(52) Landis, F. A.; March, S. R.; Deivasagayam, D.; Mathers, R. T. Crystallization of Poly(Vinylidene Fluoride) in Blends with Poly(Methyl Methacrylate-Co-Methacrylic Acid) Copolymers. *Macromol. Chem. Phys.* **2014**, *215* (2), 153−162.
(53) Salimi, A.; Yousefi, A. A. FTIR Studies of β-Phase Crystal Formation in Stretched PVDF Films. *Polym. Test.* **2003**, *22* (6), 699−704.
(54) Ramadan, K. S.; Sameoto, D.; Evoy, S. A Review of Piezoelectric Polymers as Functional Materials for Electromechanical Transducers. *Smart Mater. Struct.* **2014**, *23* (3), No. 033001.
(55) Kanik, M.; Aktas, O.; Sen, H. S.; Durgun, E.; Bayindir, M. Spontaneous High Piezoelectricity in Poly (Vinylidene Fluoride) Nanoribbons. *ACS Nano* **2014**, *8* (9), 9311−9323.
(56) Furukawa, T.; Lovinger, A. J.; Broadhurst, M. G.; Davis, G. T. Dielectric Hysteresis and Nonlinearity in a 52/48 Mol % Copolymer of Vinylidene Fluoride and Trifluoroethylene. *Macromolecules* **1983**, *16* (12), 1885−1890.
(57) Liu, Y.; Aziguli, H.; Zhang, B.; Xu, W.; Lu, W.; Bernholc, J.; Wang, Q. Ferroelectric Polymers Exhibiting Behaviour Reminiscent of a Morphotropic Phase Boundary. *Nature* **2018**, *562* (7725), 96−100.
(58) Davies, G. R.; Singh, H. Evidence for a New Crystal Phase in Conventionally Poled Samples of Poly(Vinylidene Fluoride) in Crystal Form II. *Polymer* **1979**, *20* (6), 772−774.
(59) Davis, G. T.; McKinney, J. E.; Broadhurst, M. G.; Roth, S. C. Electric-Field-Induced Phase Changes in Poly(Vinylidene Fluoride). *J. Appl. Phys.* **1978**, *49* (10), 4998−5002.
(60) Bormashenko, Y.; Pogreb, R.; Stanevsky, O.; Bormashenko, E. Vibrational Spectrum of PVDF and Its Interpretation. *Polym. Test.* **2004**, *23* (7), 791−796.
(61) Nakhmanson, S. M.; Nardelli, M. B.; Bernholc, J. Ab Initio Studies of Polarization and Piezoelectricity in Vinylidene Fluoride and BN-Based Polymers. *Phys. Rev. Lett.* **2004**, *92* (11), 115504.

https://dx.doi.org/10.1021/acsapm.0c00351
ACS Appl. Polym. Mater. 2020, 2, 3766−3780

(62) Nakhmanson, S. M.; Nardelli, M. B.; Bernholc, J. Collective Polarization Effects in β-Polyvinylidene Fluoride and Its Copolymers with Tri- and Tetrafluoroethylene. *Phys. Rev. B: Condens. Matter Mater. Phys.* **2005**, *72* (11), 115210.
(63) Teyssedre, G.; Grimau, M.; Bernes, A.; Martinez, J. J.; Lacabanne, C. α-Relaxation/Retardation Mode in Semicrystalline Polymers with Flexible Chains. *Polymer* **1994**, *35* (20), 4397−4403.
(64) Teyssedre, G.; Bernes, A.; Lacabanne, C. Influence of the Crystalline Phase on the Molecular Mobility of PVDF. *J. Polym. Sci., Part B: Polym. Phys.* **1993**, *31* (13), 2027−2034.
(65) Becker, A.; Stein, M.; Jungnickel, B. J. Dependence on Supermolecular Structure and on Charge Injection Conditions of Ferroelectric Switching of Pvdf and Its Blends with PMMA. *Ferroelectrics* **1995**, *171* (1), 111−123.

https://dx.doi.org/10.1021/acsapm.0c00351
ACS Appl. Polym. Mater. 2020, 2, 3766−3780